IEEE Photonics Journal
An IEEE Photonics Society Publication

Open Access

High-Contrast and Compact Integrated Wavelength Diplexer Based on Subwavelength Grating Anisotropic Metamaterial for 1550/2000 nm

Volume 13, Number 2, April 2021

Danfeng Zhu
Han Ye
Yumin Liu
Jing Li
Zhongyuan Yu

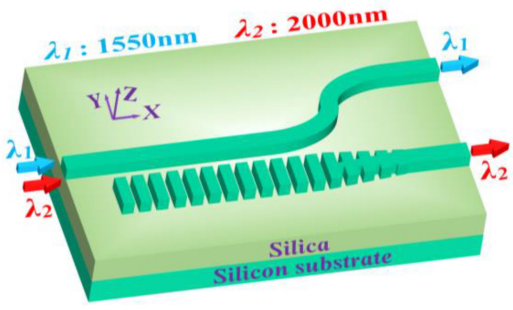

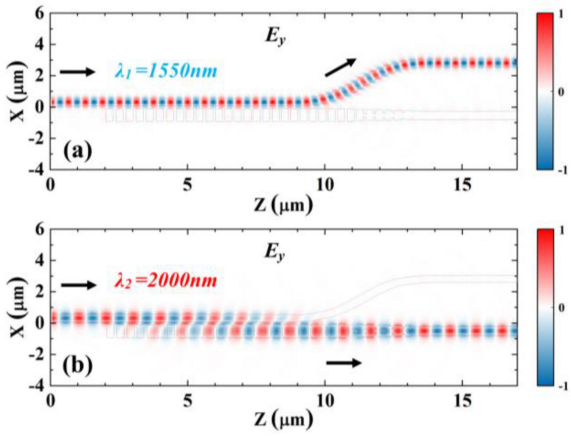

DOI: 10.1109/JPHOT.2021.3061966

High-Contrast and Compact Integrated Wavelength Diplexer Based on Subwavelength Grating Anisotropic Metamaterial for 1550/2000 nm

Danfeng Zhu, Han Ye, Yumin Liu, Jing Li, and Zhongyuan Yu

State Key Laboratory of Information Photonics and Optical Communications, Beijing University of Posts and Telecommunications, Beijing 100876, China

DOI:10.1109/JPHOT.2021.3061966

Manuscript received December 31, 2020; revised February 15, 2021; accepted February 20, 2021. Date of publication February 25, 2021; date of current version March 22, 2021. This work was supported in part by the National Natural Science Foundation of China (NSFC) under Grant 61671090 and in part by Fund of State Key Laboratory of Information Photonics and Optical Communications (Beijing University of Posts and Telecommunications), China under Grant IPOC2020ZT01. Corresponding authors: Han Ye; Yumin Liu (e-mail: Han_ye@bupt.edu.cn; Yuzhongyuan30@hotmail.com).

Abstract: A high-contrast and compact wavelength diplexer is presented for conventional 1550 nm and emerging 2000 nm based on a subwavelength-grating (SWG) coupler. The SWG silicon waveguide thoroughly blocks the light propagation around 1550 nm but fully supports 2000 nm (extinction ratio: 43.11 dB). This grating type anisotropic metamaterial not only efficiently reduces the coupling length but also expands the operational bandwidth. Simulated by 3D finite-difference time-domain method, the proposed diplexer possesses a remarkably low insertion loss and a high contrast of 25.24 (31.7) dB at 1550 (2000) nm. The operational bandwidth of 200 (108) nm is achieved with contrast over 15 dB and insertion loss below 0.22 dB. The footprint of diplexer is only 5.27 μm $\times$ 11.85 μm. Moreover, such design has the scalability by simply tuning the geometrical parameters of SWG.

Index Terms: Integrated optics, wavelength diplexer, subwavelength grating, 2 μm-waveband applications.

1. Introduction

Due to the rapidly increasing demand of optical interconnects, wavelength division multiplexing (WDM) technology has attached lots of attention, for each wavelength can load signals separately [1]. It is well known that wavelength (de)multiplexers ((de)WMUXs) are the essential building blocks of a WDM system. Generally, dual and triple (de)WMUXs are called diplexers and triplexers. It is noteworthy that several excellent properties are pursuit, e.g., low insertion loss (IL), low crosstalk (CT), high contrast (C), compactness, high robustness, and easy fabrication. Most previous researches were concentrated on the near infrared (NIR) bands (1300 – 1700 nm), especially at 1310 nm, 1490 nm, and 1550 nm, which are widely used in the fiber-to-the-X (FTTX) systems. The schemes mainly contain grating couplers [2], [3], directional couplers (DCs) [4], [5], Photonic crystals [6], [7], multimode interference (MMI) couplers [8], [9], Mach–Zehnder interferometers (MZIs) [10], inversely designed metamaterials [11], and so on. In response to the rapidly growing demand of networks, it is extremely necessary to exploit a new telecommunication window.

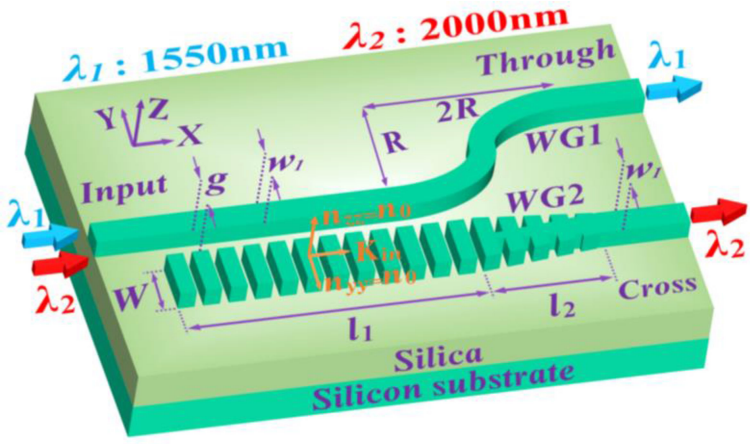

Fig. 1. Schematic of the wavelength diplexer.

In the past decades, silicon photonics of mid-infrared (MIR) (2-20 μm) has developed fast for its huge potential in biological, chemical, and industrial sensing and detection [12]–[16]. In particular, the wavelength of 2000 nm has great potential to be the new telecommunication window. It should be noted that the main building blocks working around 2000 nm have been developed, e.g., commercial lasers, hollow-core photonic bandgap fibers (HC-PBGFs) [17], modulators [18], thulium-doped fiber amplifiers (TDFAs) [19], and photodetectors [20]. After the signal light couples from a fiber to a chip, the signal light with several wavelengths needs to be processed on chip. Consequently, integrated diplexers or triplexers around 2000 nm become key components. The MMI-based diplexer was reported with reasonable performances for 1550 nm and 2000 nm [21], but it suffered from a large footprint of 6 μm $\times$ 290 μm. Further investigations need to be implemented for a compact device footprint.

As is well known, subwavelength grating (SWG) is a periodic metamaterial, whose pitch is much smaller than the wavelength of light [22]. SWG can be considered as a homogeneous anisotropic medium. SWG provides a novel freedom to control the equivalent refractive index of waveguide. A SWG DC is well established for various functionalities, e.g., frequency selection [23], [24], polarization management [25]–[28], and mode-order conversion [29], [30]. Recently, Hi *et al.* [31] proposed a scheme based on an eye-shape SWG DC with insertion loss of 0.14 dB (0.8 dB) for 1550 (2000) nm. A better performance should be pursued. Here we propose a high-contrast and compact wavelength diplexer for conventional 1550 nm and emerging 2000 nm assisted by a SWG DC. By introducing a SWG silicon waveguide, the light confinement becomes weaker and the guide-mode size effectively enlarges. Such effect will increase the coupling coefficient of SWG DC and hence reduce the coupling length. As a result, the length of this wavelength diplexer achieves a 24-fold reduction compared with Ref. [21]. To summarize, this present wavelength diplexer is quite promising with low insertion loss, high contrast, and compact footprint.

2. Design and Principle

Fig. 1 sketches the schematic of the present wavelength diplexer. It is based on the commercial silicon-on-insulator (SOI) platform with a 250-nm-silicon core and 3-μm-silica substrate. The refractive index of silicon and silica both refer to [32]. A SU8 polymer is chosen as the cladding layer with the refractive index of 1.58 [33]. This wavelength diplexer is mainly divided into two parts: waveguide 1 (WG1) and waveguide 2 (WG2). WG1 consists of a rectangle silicon waveguide and an S–bend silicon waveguide., which can prevent the crosstalk between the through port and cross port. WG2 consists of a SWG, a transitional taper and a rectangle silicon waveguide. The pitch Λ is chosen as 340 nm. In a period, the length of silicon nanowire is set as 240 nm. That is to say,

TABLE 1
Structural Parameters of the On-Chip Wavelength Diplexer

Parameters	*W*	w_1	l_1	l_2	*R*	*g*	*H*
Value (μm)	0.8	0.46	8.85	3	5	0.19	0.25

H: the thickness of the silicon waveguide.

the duty cycle δ is about 70.6%. In the transitional taper, the shortest width of trapezoidal is set as 60 nm [34]. The other geometrical parameters are listed in Table 1.

According to the ratio between λ and Λ, a periodic grating can be classed into three regimes: diffraction, Bragg reflection, and subwavelength [35], [36]. The diffraction regime is described as:

$$\frac{\lambda}{\Lambda} \leq \max\{n_c, n_s\}, \tag{1}$$

where n_c and n_s refer to the refractive indices of the cladding and substrate, λ is the free-space wavelength. When (1) is not satisfied, the diffraction effect will disappear. The Bragg reflection regime is expressed as:

$$n_B = \frac{1}{2}\lambda/\Lambda, \tag{2}$$

where n_B is the effective index of the Bloch mode. The propagation constant k_B is a constant as:

$$k_B^{Bragg} = \frac{\pi}{\Lambda}. \tag{3}$$

When the grating operates in the subwavelength regime, the effective index of the Bloch mode must satisfy:

$$n_B < \frac{1}{2}\lambda/\Lambda. \tag{4}$$

It is clear that the wavelength λ is much longer than the pitch Λ. At this time, the Bragg reflection effect will be suppressed. Assuming the grating is indefinite in the *y* and *z* directions, the grating can be modeled as a homogeneous anisotropic material (AM) with an effective refractive index tensors n_{AM} [37]:

$$n_{AM} = \mathrm{diag}[n_{xx}, n_{yy}, n_{zz}] = \mathrm{diag}[n_e, n_0, n_0], \tag{5}$$

$$n_0^2 = \delta \cdot n_{si}^2 + (1-\delta) \cdot n_{SU8}^2, \tag{6}$$

$$\frac{1}{n_e^2} = \frac{\delta}{n_{si}^2} + \frac{1-\delta}{n_{SU8}^2}, \tag{7}$$

where n_{xx}, n_{yy}, and n_{zz} refer to the components of n_{AM} in *x*-, *y*-, and *z*- directions, n_o and n_e are the ordinary and extraordinary refractive indices. The classic coupled-mode theory can be utilized to explain the principle of this SWG DC [38]. The power in WG2 is expressed as:

$$P_2(L) = P_1(0)\sin^2\left(\frac{\pi L_c(n_1 - n_2)}{\lambda}\right). \tag{8}$$

where P_1 is the power in WG1, n_1 and n_2 refer to the effective refractive indices of supermodes in the coupling region. The coupling efficiency is defined as:

$$\eta = \frac{P_2(L)}{P_1(0)}. \tag{9}$$

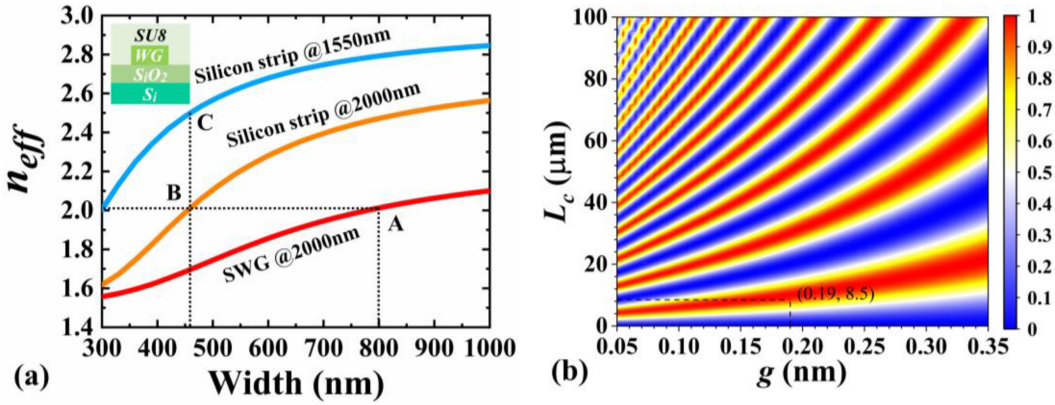

Fig. 2. (a) Effective refractive indices of the fundamental TE mode of a SU8-cladded SOI slab waveguide with varied waveguide widths. The inset illustrates the cross section of model. A (800, 2.01), B (460, 2.01), C (460, 2.5). (b) Coupling efficiencies of the SWG coupler with varied gaps and coupling length at the wavelength of 2000 nm.

Therefore, the first completely coupling length is calculated by:

$$L_c = \frac{\lambda}{2(n_1 - n_2)}. \tag{10}$$

The coupling strength dispersion coefficient D_k and the coupling strength κ are defined as:

$$D_\kappa = \frac{1}{\kappa_0} \cdot \frac{d\kappa}{d\lambda}, \tag{11}$$

$$\kappa = \frac{1}{L_c}, \tag{12}$$

where κ_0 is the coupling strength at the central wavelength.

3. Results and Discussion

As depicted in Fig. 2, we use an eigen-mode solver to calculate the effective refractive indices of the fundamental transverse electric (TE0) mode with different waveguide widths. Here the SWG is regarded as homogeneous medium with an equivalent refractive index of 2.957, which is lower than the theoretical value of 3.034 calculated by (6) because the SWG is definite in *y*- and *z*-directions. It can be observed that the slope of SWG is lower than the silicon strip at the wavelength of 2000 nm. Therefore, the introduced SWG relaxes the sensitivity of waveguide width. Similarly, this SWG also decreases the sensitivity of wavelength, which will lead to a broader operational bandwidth. In order to realize the functionality of the wavelength diplexer, the grating must operate in the Bragg reflection (subwavelength) regime at the wavelength of 1550 (2000) nm. Under these circumstances, this grating waveguide will thoroughly block the light propagation around 1550 nm but fully supports 2000 nm. According to (4), the Bragg threshold n_{BT} of this grating equal to 2.28 (2.94) at the wavelength of 1550 (2000) nm. As depicted in the black dotted lines, the width of SWG is chosen as 800 nm (point A). The effective index of grating equals to 2.01 (lower than n_{BT} of 2.94) at 2000 nm, hence the grating satisfies the subwavelength condition described in (4). To maintain the phase matching condition, the width of silicon strip is set as 460 nm (point B). At this time, the effective index of silicon strip is calculated as 2.5 at the wavelength of 1550 nm (point C). Assuming this grating operates in the subwavelength regime at 1550 nm, so it can be regarded as a homogeneous anisotropic material. Similarly, the effective index of grating should equal to 2.5 (higher than n_{BT} of 2.28) at 1550 nm, which does not satisfy the subwavelength condition described in (4). Therefore, this assumption is incorrect. Furthermore, this grating with pitch of 340

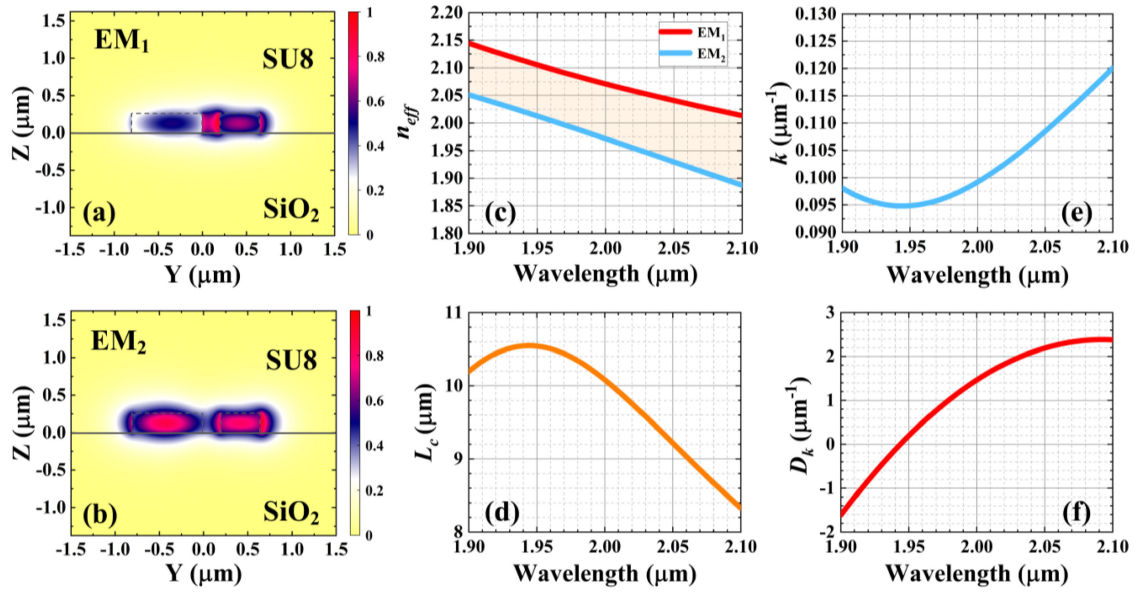

Fig. 3. The electric field profiles of (a) EM_1 and (b) EM_2. (c) Effective refractive indices of EM_1 and EM_2, (d) coupling length, (e) coupling strength, and (f) coupling strength dispersion coefficient within the bandwidth from 1.9 μm to 2.1 μm.

nm also do not fulfill the diffraction condition described in (1) at 1550 nm. It can be inferred that this grating operates in the Bragg reflection regime at 1550 nm. Consequently, the widths of SWG and WG1 are chosen to be 800 nm and 460 nm. The present SWG DC only fulfills the phase matching condition around 2000 nm but not for 1550 nm.

As depicted in Fig. 2(b), we calculate the coupling efficiencies of the SWG DC with varied gaps and coupling length according to (8) and (9). For narrow gaps of the SWG coupler, the high coupling efficiencies are more concentrated. However, they require a more precise etching process and suffers a weaker fabrication tolerance. For wider gaps, longer coupling lengths are required for the maximum coupling efficiency. To balance the above elements, we select the gap and the length of SWG as 190 nm and 850 nm, respectively. Figs. 3(a) and 3(b) illustrate the electric field profiles of the first and second Eigenmodes (EM_1 and EM_2) at the coupling region. The corresponding effective refractive indices are shown in Fig. 3(c). It can be observed that the effective refractive index difference is the smallest at the wavelength of 1944 nm. As a result, the curve of coupling length in Fig. 3(d) has a peak of 10.55 μm at the wavelength of 1944 nm calculated by (10). The theorical coupling length at the wavelength of 2 μm is calculated as 10.08 μm, which is longer than the optimized value of 8.85 μm. The SWG has weaker light confinement and bigger mode size. These effects enable the SWG to increase the coupling coefficient and reduce the coupling length. On the contrary, the coupling strength in Fig. 3(e) has valley of 0.0947 μm^{-1} at 1944 nm. Similarly, the coupling strength dispersion coefficient in Fig. 3(f) equals to 0 μm^{-1} at 1944 nm. It can be seen that the coupling strength dispersion coefficient rises as the wavelength increase, for the light of longer wavelength is easier to escape from the waveguide. Furthermore, the coupling strength dispersion coefficient achieves the peak of 2.385 μm^{-1} at the wavelength of 2092 nm.

To demonstrate above conclusions about the introduced grating, firstly, we simulate a symmetric SWG SOI wire waveguide by a three-dimension finite-difference time-domain (3D FDTD) method [39]. The mesh grids all set to 15 nm. Two 3-μm long transitional tapers are employed to suppress the coupling loss between the silicon slab waveguide and the SWG. The other geometrical parameters are the same as those in Table 1. The power flux distributions are shown in Fig. 4. When the TE0 mode at 1550 nm is incident in Fig. 4(a), the light is reflected by the SWG with a high transmittance of -0.02 dB. It is clear that little light through the SWG (only -43.13 dB). The

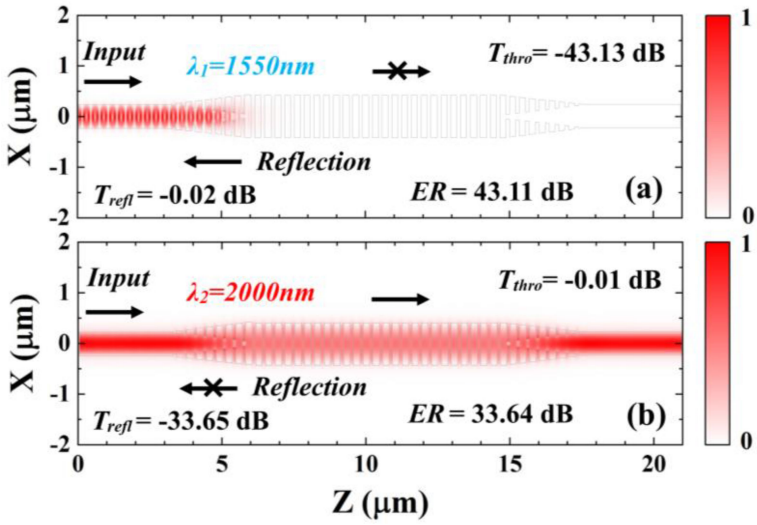

Fig. 4. Power flux distributions of the symmetric SWG SOI wire waveguide at (a) 1550 nm and (b) 2000 nm.

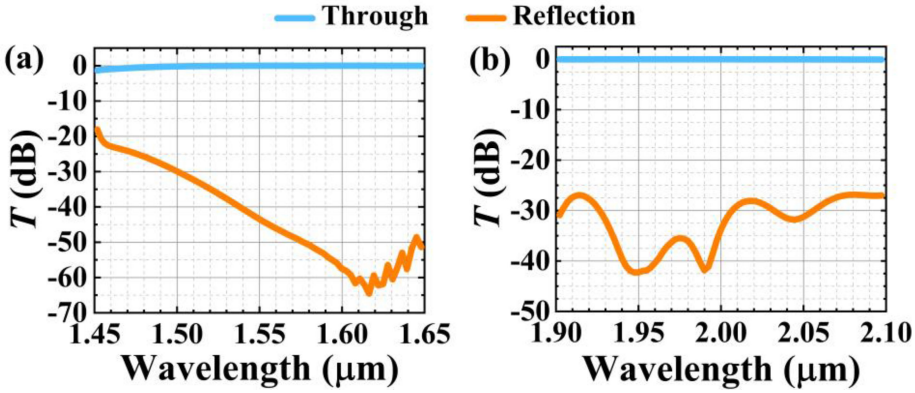

Fig. 5. Transmittance spectra of the symmetric SWG SOI wire waveguide around (a) 1550 nm and (b) 2000 nm.

extinction ratio (ER) is extremely high with 43.11 dB. Here the extinction ratio is defined as:

$$\mathrm{ER} = 10\log_{10}\left|\frac{T_{thro}}{T_{refl}}\right|. \tag{13}$$

As for the wavelength of 2000 nm in Fig. 4(b), the light propagates through the SWG with a high transmittance of -0.01 dB. The reflected transmittance is only -33.65 dB. It can be obtained a high ER of 33.64 dB. Moreover, Fig. 5 depicts the transmittance spectra with the bandwidth of 200 nm. A broad bandwidth of ER above 25 dB achieves 170 (200) nm for 1550 (2000) nm. Therefore, such SWG structure can completely separate 1550 nm and 2000 nm with a wide bandwidth over 170 nm (ER $>$ 33.65 dB). Furthermore, it can be used as an optical filter for NIR/MIR wavelengths. At this time, the middle length of SWG can be reduced to obtain a smaller device footprint.

After determining all the structural parameters of present diplexer, we characterize the performance of the wavelength diplexer by a 3D FDTD method. Fig. 6 depicts the power flux distributions of the wavelength diplexer. When the TE0 mode of 1550 nm is launched in Fig. 6(a), the grating operates in the Bragg reflection regime. Due to the huge wavevector mismatch between WG1 and the grating, the light propagates through WG1 with an exceedingly low insertion loss of 0.02 dB (transmission: 99.5%). Meanwhile, the crosstalk in WG2 is as low as -25.26 dB. A high contrast

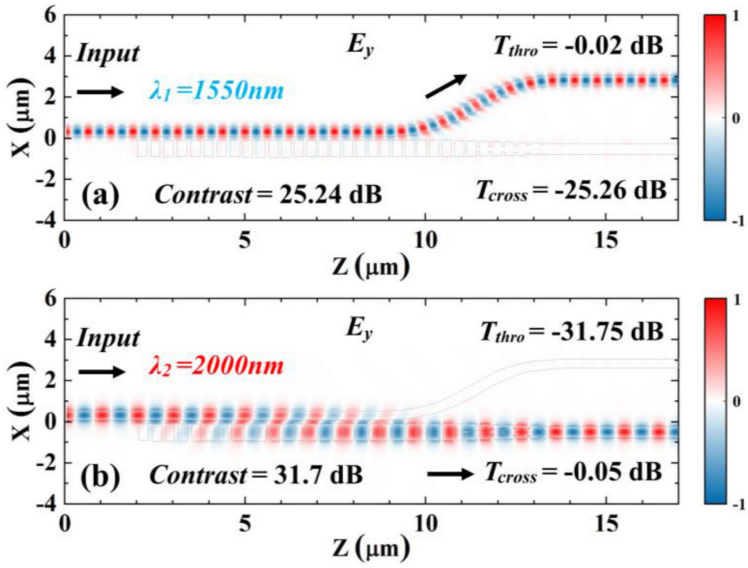

Fig. 6. Power flux distributions of the wavelength diplexer at (a) 1550 nm and (b) 2000 nm.

of 25.24 dB is achieved at 1550 nm. Here the contrast is defined as:

$$C = 10\log_{10}\left|\frac{T_{thro}}{T_{cross}}\right| \tag{14}$$

The case of 2000 nm in Fig. 6(b) is contrary. Because the grating operates in the subwavelength regime, it can be considered as a homogeneous medium with an effective refractive index of 2.96. It is a little smaller than the theoretical value of 3.02 calculated by (6), for the SWG is limited in the y and z directions. Due to the satisfied phase-matching condition, the light propagates through WG2 with a low insertion loss of 0.05 dB (transmission: 98.8%). Moreover, the crosstalk in WG1 is extremely low with only −31.75 dB. It is clear that such wavelength diplexer obtains a remarkably high contrast of 31.7 dB at 2000 nm.

We also characterize the transmittance spectra responses within 200 nm bandwidth. As depicted in Figs. 7(a) and 7(b), the present diplexer displays an excellent performance with insertion loss below 0.19 dB, crosstalk below −20.03 dB, and contrast over 19.84 dB from 1450 nm to 1650 nm. A broadband of over 200 nm around 1550 nm is achieved because of the huge wavevector mismatch. Figs. 7(c) and 7(d) depict the device performances for the wavelength from 1900 nm to 2100 nm. The insertion loss and crosstalk keep below 0.22 dB and −15.35 dB from 1942 nm to 2050 nm. In this 108 nm bandwidth, the peak of contrast is at the wavelength of 1994 nm with 37.39 dB. In short, the present diplexer has a working bandwidth of 200 (108) nm around the wavelength of 1550 (2000) nm, respectively. The present design is better than the one in Ref. [31] theoretically. When the TE0 mode at 1550 nm is incident, the light propagates only in the upper waveguide. The SWG in lower waveguide has little influence to the propagation of 1550-nm light. In Ref. [31], the light couples from the upper waveguide to the lower waveguide. However, the middle SWG unavoidably causes tiny reflection or diffraction. As for the wavelength of 2000 nm, the light couples from the upper waveguide to the lower waveguide. However, the light in Ref. [31] couples from the upper waveguide to the lower waveguide, and then couples back to the upper waveguide. Such twice coupling in the SWG causes more loss. Table 2 shows the performances of the proposed structure and previous designs.

This diplexer can be fabricated on a SOI wafer with 250-nm-thick silicon layer and 3-μm silica buried oxide. Both electron beam lithography (EBL) and inductively coupled plasma (ICP) etching are required to perform the exposure and etching process. A 1 μm-thick SU8 polymer cladding

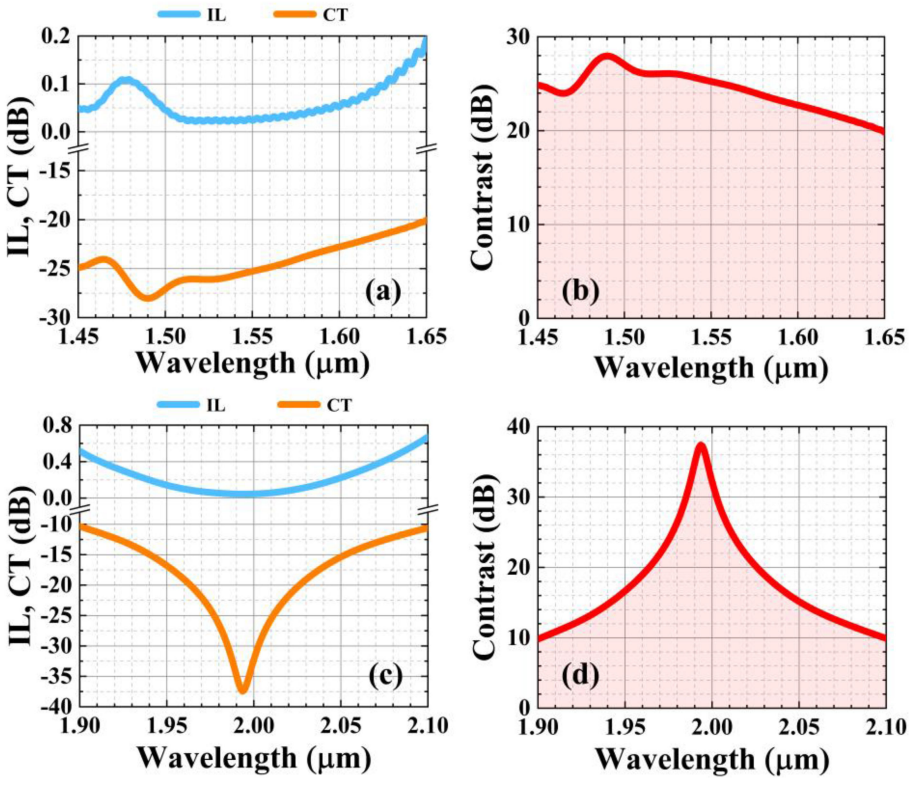

Fig. 7. Transmittance spectra of the wavelength diplexer. (a) Insertion loss, crosstalk and (b) contrast around 1550 nm. (c) Insertion loss, crosstalk and (d) contrast around 2000 nm.

TABLE 2

Comparison of the On-Chip Wavelength Diplexers for 1550 Nm and 2000 nm. The Performances are Simulated By 3D FDTD Method

Reference	Structure	Fab.	Footprint (μm^2)	Ch. 1550 nm			Ch. 2000 nm		
				T	C (dB)	BW (C>15 dB)	T	C (dB)	BW (C>15 dB)
21	MMI	√	6 × 290	~97%	19.83	–	~76%	19.42	–
31	SWG DC	–	2.5 × 13.9	~97%	27.5	112	~84%	24.7	102
This	SWG DC	–	5.27 × 11.85	>99%	25.24	200	>98%	31.7	108

T refers to the transmission efficiency.

layer should be spun to cover the device. As reported in Ref. [28] and [37], SWG with feature size below 100 nm has been realized. Here we survey the fabrication tolerance with deviation of SWG segment as illustrated in Fig. 8. The pitch Λ remains as a constant of 340 nm. We assume that the variations of SWG segment are all the same. It can be observed that the device performance is robuster at 1550 nm than 2000 nm. Fig. 8(a) depicts that the contrast keeps over 20.04 dB within the 20 nm-variation range at 1550 nm. The contrast shows a higher fluctuation at 2000 nm as illustrated in Fig. 8(b). This diplexer retains contrast above 15 dB only within a 6 nm-variation range. Because the light of 2000 nm couples from the upper waveguide to the lower SWG waveguide, and the light of 1550 nm only propagates in the upper waveguide. The present structure must strictly satisfy the phase matching condition. To address this issue, there may be two solutions according to Ref. [27].

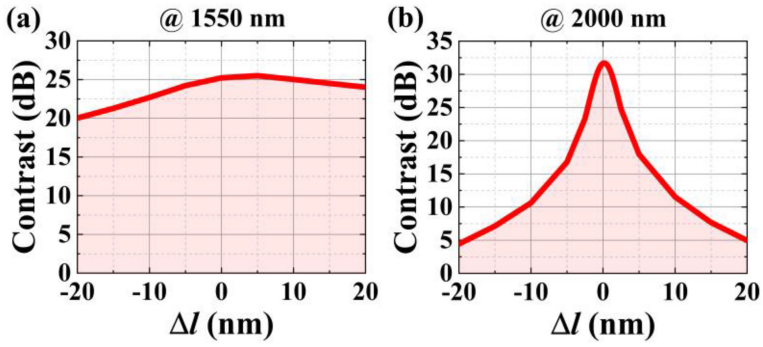

Fig. 8. Contrast with variations of the SWG segment at (a) 1550 nm and (b) 2000 nm.

One is introducing SWGs in both upper and lower waveguides. The other is introducing a silicon strip waveguide between upper and lower waveguides.

To study the scalability of this wavelength diplexer, the conventional wavelengths of 1310 nm and 1490 nm are separately launched into the device. The output transmittances through WG1 and WG2 achieve −0.03 dB and −32.89 dB (−0.08 dB and −30.35 dB) for 1310 (1490) nm. They are both similar to 1550 nm with an ultrahigh through transmittance (T_{thro}) and an ultralow cross transmittance (T_{cross}). Consequently, such diplexer can be compatible perfectly with the reported diplexers and triplexers working around 1310 nm, 1490 nm, and 1550 nm by cascading them. This diplexer is arranged in the first position to process the light around 2000 nm. More importantly, such structure can be expanded to the (de)WMUXs for 1310 nm and 1490 nm just by tuning the geometrical parameters of grating to satisfy the phase matching condition.

4. Conclusion

In summary, we propose and demonstrate a wavelength diplexer around 1550 nm and 2000 nm based on a SWG DC. The grating respectively operates in the Bragg reflection and the subwavelength regimes around these two wavelengths. This device exhibits an excellent performance with low insertion loss and high contrast of 25.24 (31.7) dB for 1550 (2000) nm. A working bandwidth is achieved larger than 200 (108) nm. What' more, the device length is only 11.85 μm. More importantly, such device not only is perfect compatible with the reported diplexers and triplexers but also has the scalability by tuning the structural parameters of subwavelength grating. We hope such design could be helpful to on-chip 2 μm-waveband applications and the future FTTX systems.

Disclosures

The authors declare no conflicts of interest.

References

[1] A. Liu *et al.*, "Wavelength division multiplexing based photonic integrated circuits on silicon-on-insulator platform," *IEEE J. Sel. Topics Quantum Electron.*, vol. 16, no. 1, pp. 23–32, Jan./Feb. 2010.
[2] D. Liu, M. Zhang, and D. Dai, "Low-loss and low-crosstalk silicon triplexer based on cascaded multimode waveguide gratings," *Opt. Lett.*, vol. 44, no. 6, pp. 1304–1307, 2019.
[3] J. Chen, Y. Zhang, and Y. Shi, "An on-chip triplexer based on silicon Bragg grating-assisted multimode interference couplers," *IEEE J. Photon. Technol. Lett.*, vol. 29, no. 1, pp. 63–65, Jan. 2017.
[4] Y. Shi, S. Anand, and S. He, "Design of a polarization insensitive triplexer using directional couplers based on submicron silicon rib waveguides," *J. Lightw. Technol.*, vol. 27, no. 11, pp. 1443–1447, 2009.
[5] J. Chen and Y. Shi, "An ultracompact silicon triplexer based on cascaded bent directional couplers," *J. Lightw. Technol.*, vol. 35, no. 23, pp. 5260–5264, 2017.
[6] L. Xu *et al.*, "Broadband 1310/1550 nm wavelength demultiplexer based on a multimode interference coupler with tapered internal photonic crystal for the silicon-on-insulator platform," *Opt. Lett.*, vol. 44, no. 7, pp. 1770–1773, 2019.

[7] O. M. Nawwar, H. M. H. Shalaby, and R. K. Pokharel, "Photonic crystal-based compact hybrid WDM/MDM (De)multiplexer for SOI platforms," *Opt. Lett.*, vol. 43, no. 17, pp. 4176–4179, 2018.
[8] J. Xiao, X. Liu, and X. Sun, "Design of an ultracompact MMI wavelength demultiplexer in slot waveguide structures," *Opt. Exp.*, vol. 15, no. 13, pp. 8300–8308, 2007.
[9] L. Liu, Q. Deng, and Z. Zhou, "An ultra-compact wavelength diplexer engineered by subwavelength grating," *IEEE J. Photon. Technol. Lett.*, vol. 29, no. 22, pp. 1927–1930, Nov. 2017.
[10] N. N. Feng *et al.*, "Low-loss polarization-insensitive silicon-on-insulator-based WDM filter for triplexer applications," *IEEE Photon. Technol. Lett.*, vol. 20, no. 23, pp. 1968–1970, Dec. 2008.
[11] A. Y. Piggott, J. Lu, K. G. Lagoudakis, J. Petykiewicz, T. M. Babinec, and J. Vuckovic, "Inverse design and demonstration of a compact and broadband on-chip wavelength demultiplexer," *Nat. Photon.*, vol. 9, no. 6, pp. 374–37, 2015.
[12] F. Sun, B. Dong, J. Wei, Y. Ma, H. Tian, and C. Lee, "Demonstration of mid-infrared slow light one-dimensional photonic crystal ring resonator with high-order photonic bandgap," *Opt. Exp.*, vol. 28, no. 21, pp. 30736–30747, 2020.
[13] M. Mahmud, D. Rosenmann, D. Czaplewski, J. Gao, and X. Yang, "Chiral plasmonic metasurface absorbers in the mid-infrared wavelength range," *Opt. Lett.*, vol. 45, no. 19, pp. 5372–5375, 2020.
[14] J. Xu *et al.* "Nanometer-scale heterogeneous interfacial sapphire wafer bonding for enabling plasmonic-enhanced nanofluidic mid-infrared spectroscopy," *ACS Nano*, vol. 14, no. 9, pp. 12159–12172, 2020.
[15] M. Pi *et al.* "Theoretical study of microcavity-enhanced absorption spectroscopy for mid-infrared methane detection using a chalcogenide/silica-on-fluoride horizontal slot-waveguide racetrack resonator," *Opt. Exp.*, vol. 28, no. 15, pp. 21432–21446, 2020.
[16] H. Wang, E. Janzen, L. Wang, and J. Edgar, "Probing mid-infrared phonon polaritons in the aqueous phase," *Nano Lett.*, vol. 20, no. 5, pp. 3986–3991, 2020.
[17] P. J. Roberts *et al.*, "Ultimate low loss of hollow-core photonic crystal fibres," *Opt. Exp.*, vol. 13, no. 1, pp. 236–244, 2005.
[18] W. Cao *et al.*, "High-speed silicon modulators for the 2 μm wavelength band," *Optica*, vol. 5, no. 9, pp. 1055–1062, 2018.
[19] Z. Li *et al.* "Diode-pumped wideband thulium-doped fiber amplifiers for optical communications in the 1800-2050 nm window," *Opt. Exp.*, vol. 21, no. 22, pp. 26450–26455, 2013.
[20] Y. Chen, Z. Xie, J. Huang, Z. Deng, and B. Chen, "High-speed uni-traveling carrier photodiode for 2 μm wavelength application," *Optica*, vol. 6, no. 7, pp. 884–889, 2019.
[21] M. S. Rouifed *et al.*, "Ultra-compact MMI-based beam splitter demultiplexer for the NIR/MIR wavelengths of 1.55 μm and 2 μm," *Opt. Exp.*, vol. 25, no. 10, pp. 10893–10900, 2017.
[22] P. Cheben, R. Halir, J. H. Schmid, H. A. Atwater, and D. R. Smith, "Subwavelength integrated photonics," *Nature*, vol. 560, no. 7720, pp. 565–572, 2018.
[23] P. Yeh and H. F. Taylor, "Contradirectional frequency-selective couplers for guided-wave optics," *Appl. Opt.*, vol. 19, no. 16, pp. 2848–2855, 1980.
[24] W. Shi, X. Wang, W. Zhang, L. Chrostowski, and N. A. F. Jaeger, "Contradirectional couplers in silicon-on-insulator rib waveguides," *Opt. Lett.*, vol. 36, no. 20, pp. 3999–4001, 2011.
[25] Y. Xiong, J. G. Wangüemert-Pérez, D. X. Xu, J. H. Schmid, P. Cheben, and W. N. Ye, "Polarization splitter and rotator with subwavelength grating for enhanced fabrication tolerance," *Opt. Lett.*, vol. 39, no. 24, pp. 6931–6934, 2014.
[26] Y. Wang *et al.*, "Ultra-compact sub-wavelength grating polarization splitter-rotator for silicon-on-insulator platform," *IEEE Photon. J.*, vol. 8, no. 6, Dec. 2016, Art. no. 7805709.
[27] J. M. Luque-González *et al.*, "Polarization splitting directional coupler using tilted subwavelength gratings," *Opt. Lett.*, vol. 45, no. 13, pp. 3398–3401, 2020.
[28] M. Ma *et al.*, "Sub-wavelength grating-assisted polarization splitter-rotators for silicon-on-insulator platforms," *Opt. Exp.*, vol. 27, no. 13, pp. 17581–17591, 2019.
[29] Y. He *et al.*, "Silicon high-order mode (de)multiplexer on single polarization," *J. Lightw. Technol.*, vol. 36, no. 24, pp. 5746–5753, 2018.
[30] Y. He, Y. Zhang, H. Wang, L. Sun, and Y. Su, "Design and experimental demonstration of a silicon multi-dimensional (de)multiplexer for wavelength-, mode- and polarization-division (de)multiplexing," *Opt. Lett.*, vol. 45, no. 10, pp. 2847–2849, 2020.
[31] B. Hi and J. Xiao, "Ultracompact silicon-based wavelength diplexer for 1.55/2 μm using subwavelength gratings," *Opt. Lett.*, vol. 44, no. 11, pp. 2775–2778, 2019.
[32] E. D. Palik, *Handbook of Optical Constants of Solids*, New York, NY, USA: Academic, 1985.
[33] J. H. Schmid *et al.* "Temperature-independent silicon subwavelength grating waveguides," *Opt. Lett.*, vol. 36, no. 11, pp. 2110–2112, 2011.
[34] Z. Jafari, A. Zarifkar, and M. Miri, "Compact fabrication-tolerant subwavelength-grating-based two-mode division (de)multiplexer," *Appl. Opt.*, vol. 56, no. 26, pp. 7311–7319, 2017.
[35] R. Halir *et al.*, "Waveguide sub-wavelength structures: A review of principles and applications," *Laser Photon. Rev.*, vol. 9, no. 1, pp. 25–49, 2015.
[36] R. Halir *et al.*, "Subwavelength-grating metamaterial structures for silicon photonic devices," *Proc. IEEE*, vol. 106, no. 12, pp. 2144–2157, Dec. 2018.
[37] H. Xu, D. Dai, and Y. Shi, "Ultra-broadband and ultra-compact on-chip silicon polarization beam splitter by using hetero-anisotropic metamaterials," *Laser Photon. Rev.*, vol. 13, no. 4, 2019, Art. no. 1800349.
[38] A. Yariv, "Coupled-mode theory for guided-wave optics," *IEEE Quantum Electron.*, vol. QE-9, no. 9, pp. 919–933, Sep. 1973.
[39] D. M. Sullivan, *Electromagnetic Simulation Using the FDTD Method*, New York, NY, USA: IEEE, 2000.